

Subcoercive-field dielectric response of $0.5(\text{Ba}_{0.7}\text{Ca}_{0.3}\text{TiO}_3)-0.5(\text{BaZr}_{0.2}\text{Ti}_{0.8}\text{O}_3)$ thin film: peculiar third harmonic signature of phase transitions and residual ferroelectricity

Kevin Nadaud^{1, a)}, Guillaume F. Nataf¹, Nazir Jaber¹, Micka Bah¹, Béatrice Negulescu¹, Pascal Andrezza², Pierre Birnal² and Jérôme Wolfman¹

¹⁾ GREMAN UMR 7347, Université de Tours, CNRS, INSA-CVL, 16 rue Pierre et Marie Curie, 37071 Tours, France

²⁾ ICMN, CNRS, Université d'Orléans, 1b rue de la Férollerie, CS 40059, 45071 Orléans Cedex 02, France

Sub-coercive field non-linearities in $0.5(\text{Ba}_{0.7}\text{Ca}_{0.3}\text{TiO}_3)-0.5(\text{BaZr}_{0.2}\text{Ti}_{0.8}\text{O}_3)$ (BCTZ 50/50) thin film elaborated using pulsed laser deposition are studied using permittivity and phase angle of the third harmonic measurements as function of the AC measuring field E_{AC} and temperature. The global phase transition temperature T_{max} for which the permittivity is maximum, decreases from 330 K to 260 K when E_{AC} increases. Rayleigh analysis of the AC field dependence of the relative permittivity shows a regular decrease of the domain wall motion contributions as temperature increases up to T_{max} and an even more pronounced decrease above T_{max} . This measurement reveals that the ferroelectric behavior subsists 70 K above the global phase transition. The phase angle of the third harmonic at temperatures below 275 K, is characteristic of a conventional ferroelectric and from 275 K to $T_{max} = 330$ K of a relaxor. Above T_{max} , the thin film exhibits a peculiar phase angle of the third harmonic, which consists of $-180^\circ \rightarrow -225^\circ \rightarrow +45^\circ \rightarrow 0^\circ$ instead of the $-180^\circ \rightarrow -90^\circ \rightarrow 0^\circ$ found for relaxor. This peculiar behavior is observed only on heating, and is tentatively attributed to changes in the correlations between polar nanoregions.

Keywords: Impedance spectroscopy, hyperbolic analysis, relaxor, domain wall

Relaxor ferroelectrics are promising materials for energy storage devices and actuators thanks to their high dielectric permittivity and high piezoelectric coefficients^{1,2}. In this context, BaTiO₃-based materials such as the $\text{Ba}_{1-x}\text{Ca}_x\text{Ti}_{1-y}\text{Zr}_y\text{O}_3$ (BCTZ) solid solution represent an interesting alternative to lead-based materials³⁻⁶. Their properties are strongly linked to the dynamics of domain walls, in their ferroelectric phases, that can enhance the electromechanical response but also significantly increase losses⁷⁻⁹. In addition, they exhibit polar nanoregions (PNRs), clusters in which the polarization is randomly aligned in absence of external electric field¹⁰⁻¹³, that contribute significantly to the macroscopic dielectric and piezoelectric responses¹⁴⁻¹⁶.

Those PNRs can subsist several kelvins above the Curie temperature (in the centrosymmetric phase)¹⁷⁻¹⁹ and are visible in the non-linear response of the materials, similar to the signature of domain walls in conventional ferroelectrics^{13,20,21}. On cooling from the paraelectric phase, relaxor ferroelectrics can be described through three key temperatures^{15,22}: (1) the Burns temperature T_B where the population of PNRs begins to be significant²³, (2) the freezing temperature T_f where the PNRs have grown such that they become static²⁴, (3), the depolarization temperature T_d where long-range

ferroelectric domains can be achieved by electric-field poling^{25,26}, induced by the percolation of PNRs²⁷.

In this article, we study the phase transitions in a thin film of BCTZ 50/50 using the relative permittivity at the first harmonic (using hyperbolic law) and the evolution of phase angle of the third harmonic as a function of the AC field for different temperatures. Using hyperbolic analysis, we show that residual ferroelectricity persists up to 70 K above the maximum in permittivity indicating the transition to the cubic phase. Above this temperature, a faster decay of the reversible and irreversible domain wall motion contributions is visible. The crossing of this temperature is also well visible on the phase angle of the third harmonic, which exhibits a totally different evolution with increasing AC field below and above it.

At sub-switching AC fields, for a homogeneous distribution of pinning centers, the relative permittivity can be described using the Rayleigh law:^{28,29}

$$\varepsilon_r = \varepsilon_{r-l} + \alpha_r E_{AC} \quad (1)$$

Where E_{AC} corresponds to the magnitude of the applied measuring electric field, ε_{r-l} is the lattice contribution to the permittivity, α_r is the irreversible contribution from the motion of domain walls (domain wall pinning/unpinning), polar cluster boundaries, or phase boundaries and corresponds to the slope of the permittivity v.s. electric field curve. In such conditions of homogeneous distribution of pinning centers, the polarization versus electric field loop can be described using the following expression:^{20,28}

$$P = \varepsilon_0 (\varepsilon_{r-l} + \alpha_r E_0) E \pm \frac{\varepsilon_0 \alpha_r}{2} (E_0^2 - E^2) + \dots \quad (2)$$

^{a)} Author to whom correspondence should be addressed: kevin.nadaud@univ-tours.fr

The following article has been submitted to Applied Physics Letters. After it is published, it will be found at <https://dx.doi.org/10.1063/5.0182718>

The sign + stands for the decreasing and the sign – for the increasing part of the AC field. The second term reflects the hysteretic contribution of domain walls to the polarization. This non-linear expression of the polarization gives the following Fourier series decomposition when the applied electric field is $E(t) = E_0 \sin(\omega t)$:³⁰

$$P(t, E_0) = \varepsilon_0 (\varepsilon_{r-l} + \alpha_r E_0) E_0 \sin(\omega t) + \sum_{1,3,5,\dots} \frac{4\varepsilon_0 \alpha_r E_0^2 \sin\left(\frac{\pi n}{2}\right)}{\pi n(n^2 - 4)} \cos(n\omega t) \quad (3)$$

The irreversible domain wall motion contribution is thus out-of-phase with the measuring electric field in the case of an ideal material. In order to describe a real material, equation (2) can contain additional terms, reflecting the degree of randomness of the energy profile,²¹ and in that case, harmonics may not be purely out-of-phase. For this reason, the non-linear response of a relaxor or a ferroelectric material can be investigated by extracting the phase of the third-harmonic contribution to the polarization and its evolution with the measuring field amplitude, which gives information on the hysteretic or non-hysteretic character of domain wall motions^{13,20,21,31,32}.

In a real material, the distribution of pinning centers is not homogeneous and for low AC fields, the relative permittivity is almost constant, corresponding to reversible domain wall contributions, also called domain wall vibration^{29,33}. A generalized expression can then be used to describe the permittivity evolution, called the hyperbolic law:³⁴⁻³⁶

$$\varepsilon_r = \varepsilon_{r-l} + \sqrt{\varepsilon_{r-rev}^2 + (\alpha_r E_{AC})^2} \quad (4)$$

with ε_{r-rev} the reversible domain wall motion contribution, proportional to the domain wall density³⁷⁻³⁹. ε_{r-l} , ε_{r-rev} and α_r can be obtained by measuring the relative permittivity as a function of the driving field. Their evolution with driving frequency, temperature, DC bias field or previous states, allows understanding dielectric relaxations⁴⁰, residual ferroelectricity¹⁸, contributions to tunability^{41,42} and annealing/cycling effects^{32,38}.

Irreversible domain wall motions make the relative permittivity AC field dependent, which is critical in many application⁴³ especially because it can subsist in the microwave frequency range⁴⁴.

Polycrystalline 380 nm thick BCTZ film has been grown on Pt/TiO₂/MgO substrate by pulsed laser deposition. Details on growth conditions can be found in the supplementary information. Top circular Au/Ti electrodes (150 μm radius) were deposited through a shadow mask. The metal-insulator-metal topology has been chosen for the simple extraction of the dielectric properties using the parallel plate capacitor formula.

X-ray diffraction (see diffraction pattern in Fig. S1 of supplementary information) shows that the BCTZ film is single-phased and polyoriented. Peak positions could be indexed according to orthorhombic BCTZ 50/50 (pdf

#04-022-8189). The film composition has been characterized by Rutherford Back Scattering (RBS, see Figure S2a,b) and was found to be close to the nominal target composition (see table S1).

The single frequency Vertical Piezoresponse Force Microscopy (VPFM) is used to map the electrical polarization at nanoscale in the BCTZ film. A SCM-PTSI tip with a spring constant of 2.8 N m⁻¹ and a radius of curvature of 15 nm is mounted on the probe holder. An AC amplitude of 0.5 V at a drive frequency of 327 kHz (i.e. the contact resonance frequency) is applied to the BCTZ sample while the tip is grounded. The scan size and the scan rate are set to 500 nm and 0.2 Hz, respectively.

The dielectric characterizations presented in this article have been acquired using a lock-in amplifier (MFLI with MD option, Zurich Instrument) connected to a temperature-controlled probe station (Summit 12000, Cascade Microtech). The AC measuring signal has been generated using the embedded lock-in generator. Its amplitude has been swept from 10 mV_{rms} to 1 V_{rms} at a frequency of 10 kHz. The applied voltage and current through the capacitor are measured simultaneously by the lock-in. The first harmonic of the voltage, in addition to first, second and third harmonics of the current, are demodulated simultaneously. $|V| \exp(j\theta_V)$ is the phasor representing the applied voltage and $|I_k| \exp(j\theta_{I_k})$ the phasor representing the k -th harmonic of the current (with j the imaginary unit). The first harmonic of the current and the applied voltage are used to compute the complex impedance:^{32,35,45}

$$Z = \frac{|V|}{|I_1|} \exp(j(\theta_V - \theta_{I_1})) \quad (5)$$

The complex capacitance C^* can hence be derived from the complex impedance:

$$C^* = \frac{1}{j\omega Z} = \frac{|I_1|}{\omega|V|} \exp\left(j\left(\theta_{I_1} - \theta_V - \frac{\pi}{2}\right)\right) \quad (6)$$

ω the angular frequency of the measuring voltage. The material relative permittivity ε_r^* :

$$\varepsilon_r^* = \frac{t}{S\varepsilon_0} C^*, \quad (7)$$

with t the thickness of the film, S the surface of the electrodes and ε_0 the vacuum permittivity. In the present case, the electrodes are sufficiently thick in order to limit the effect of the series resistance on the measured impedance.

In addition to the measurement as a function of the AC amplitude, the relative permittivity has been measured from 31 Hz to 31 kHz with an AC amplitude of 40 mV_{rms}.

The k -th harmonic phase angle extraction process is similar and its value can be obtained using the following expression:³²

$$\delta_k = \theta_{I_k} - k\theta_V - \frac{\pi}{2} \quad (8)$$

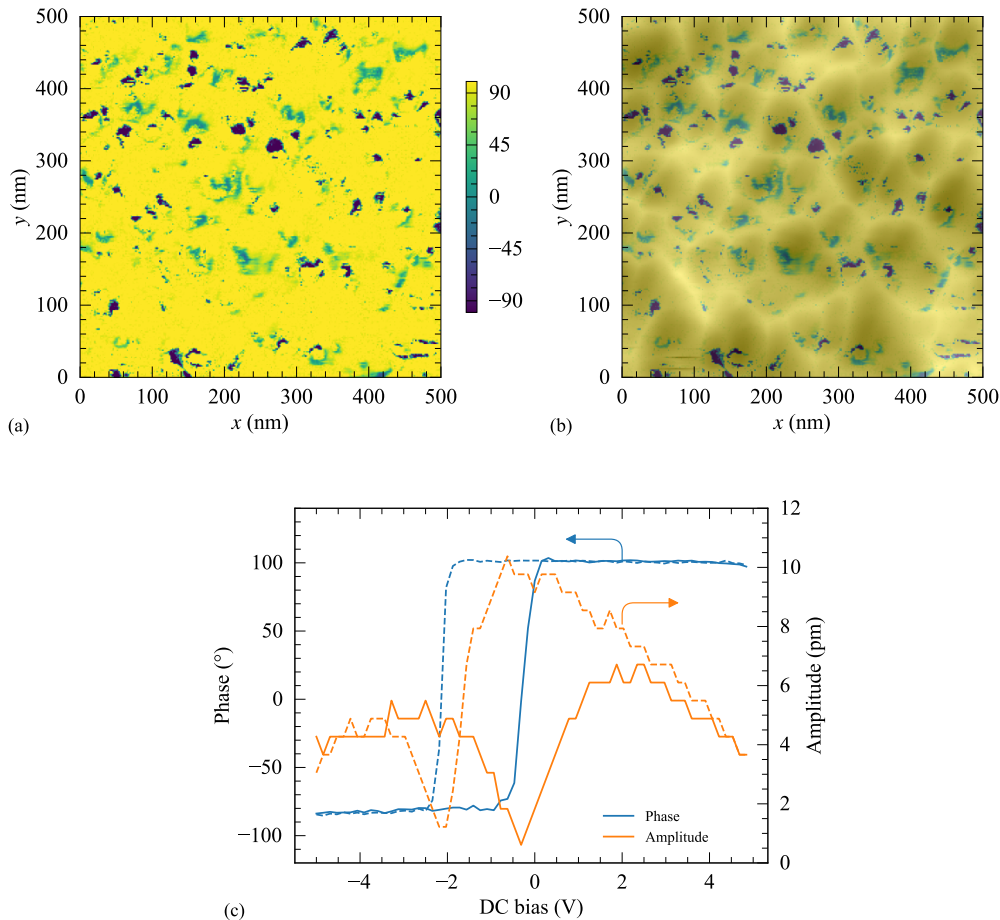


Figure 1. Phase of the Vertical PFM (VPFM) (a). Superimposition of the phase signal and the topography (b). PFM phase and amplitude as a function of an applied DC voltage V_{DC} (c).

Fig. 1a displays the PFM phase, associated with the domain orientation (up or down). It highlights that the majority of the grains in the thin film form a single domain in the out-of-plane projection of the electrical polarization. Nevertheless, few grains present a polydomain configuration, as the superimposition of the topography one and that of the PFM phase shows (see dark and bright colors in Fig. 1b). Fig. 1c displays the PFM phase and amplitude signals as a function of DC bias. These piezoresponse data are a signature of ferroelectric behavior. A phase difference of 182° between the up and down domains is observed at the coercive voltage ($|V_c| \simeq 1$ V). At the same time, the PFM amplitude drops as the polarization switching under the tip gradually takes place. Topography measurement using AFM is given in supplementary material.

Fig. 2a shows the relative permittivity as a function of temperature for different frequencies. T_{max} have been determined from a least square fitting of ϵ'_r with a parabola⁴⁶. The decrease of the permittivity when the frequency increases is stronger for low temperatures (be-

low 300 K) than for high temperatures (above 340 K). This results in a shift of the maximum permittivity temperature T_{max} with frequency (Fig. 2b), typical of relaxor-ferroelectrics behavior^{12,15}. The relaxor behavior is confirmed by the $P(E)$ loop and the analysis of the phase transition diffuseness, using modified Curie-Weiss analysis, both in supplementary material (Fig. S4 and S5).

Fig. 2c shows the relative permittivity as a function of temperature for different values of the AC measuring field. For an AC field of 0.4 kV cm^{-1} , T_{max} is 330 K, i.e. slightly lower than that reported for bulk BCTZ ceramics in the literature (363 K⁴⁷, 365 K⁴⁸, 373 K⁴⁹) but very similar to the one obtained for thin films: 323 K^{50,51}. An inflection point is also visible, at 270 K, and may correspond to a structural transition. It is close to the tetragonal-orthorhombic and orthorhombic-rhombohedral transition temperatures observed in bulk ceramics⁵² and matches with anomalies observed in pyroelectric current⁵³ and dielectric and elastic properties⁴⁷. Bulk $0.5(\text{Ba}_{0.7}\text{Ca}_{0.3}\text{TiO}_3) - 0.5(\text{BaZr}_{0.2}\text{Ti}_{0.8}\text{O}_3)$ (BCTZ 50/50) is cubic (Pm-3m) above 360 K. On cooling, it

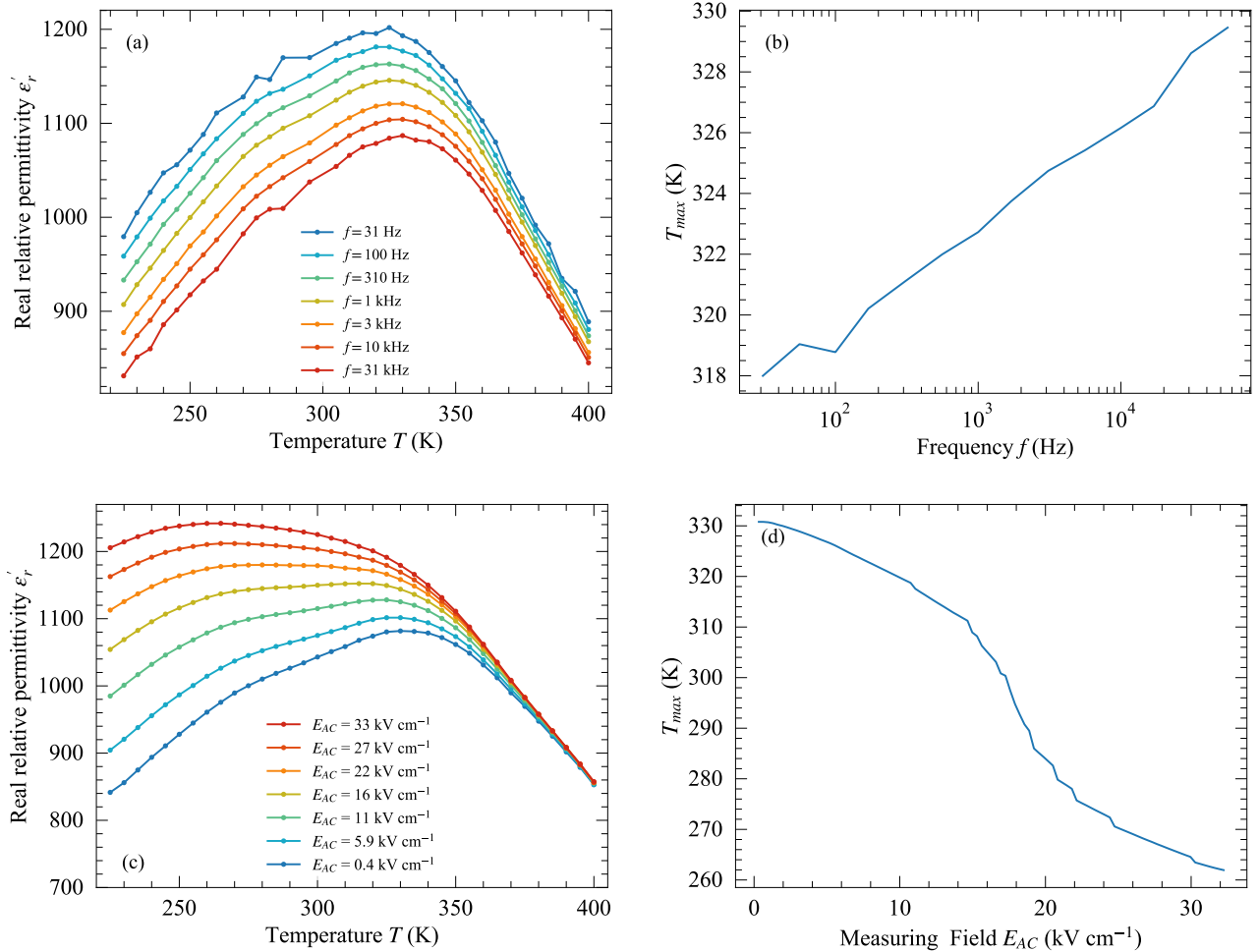


Figure 2. Relative permittivity as a function of the temperature for different measurement frequency for $E_{AC} = 1.2 \text{ kV cm}^{-1}$ (a). T_{max} for which the relative permittivity is maximum as a function of the frequency for $E_{AC} = 1.2 \text{ kV cm}^{-1}$ (b). Relative permittivity as a function of the temperature for different values of the AC measuring field for $f = 10 \text{ kHz}$ (c). T_{max} for which the relative permittivity is maximum as a function of the AC measuring field for $f = 10 \text{ kHz}$ (d).

enters a tetragonal phase (P4mm), that coexist with a rhombohedral phase (R3m) between 310 K and 210 K. Below 210 K, it is rhombohedral⁵².

When the AC measuring field increases, the relative permittivity increases due to irreversible contributions from the motion of domain walls, polar cluster boundaries, or phase boundaries^{54–56}. One can note that the lower the temperature, the higher the increase of the relative permittivity with AC field. The consequence of this increase is a shift towards lower temperatures of the temperature where the relative permittivity is maximum (T_{max}) when the AC field increases (Fig. 2d). Thus, in the following, the estimation of the maximum of the permittivity T_{max} indicative of the transition to the cubic phase, is conducted at low AC field, to reduce the influence of domain wall motion.

The measurement has also been performed for decreasing temperature (400 K \rightarrow 225 K) and presented in supplementary material (Fig. S5). The permittivity exhibits

higher values and a maximum at a slightly lower temperature (320 K) compared to increasing temperatures (330 K).

Fig. 3 shows the relative permittivity variation $\Delta\epsilon'_r = \epsilon'_r - \epsilon'_r(0)$ and the phase angle of the third harmonic, as a function of the AC measuring field amplitude and for different temperatures, on heating. $\Delta\epsilon'_r$ increases when the AC field increases, due to the irreversible domain wall motion contribution. This increase is stronger at low temperatures (Fig. 3a, 3c). The increase in permittivity vs AC field persists above T_{max} (black dashed line), corresponding to residual ferroelectricity, similar to what has been observed in (Ba, Sr)TiO₃^{17,18,57}. Similar trends are observed when the measurement is performed on cooling (Fig. 3e, 3g).

Fig. 3b shows the phase angle of the third harmonic as a function of the AC measuring field, for different temperatures, on heating. At low temperatures, up to 275 K, the evolution of the phase-angle is typical of soft or weakly

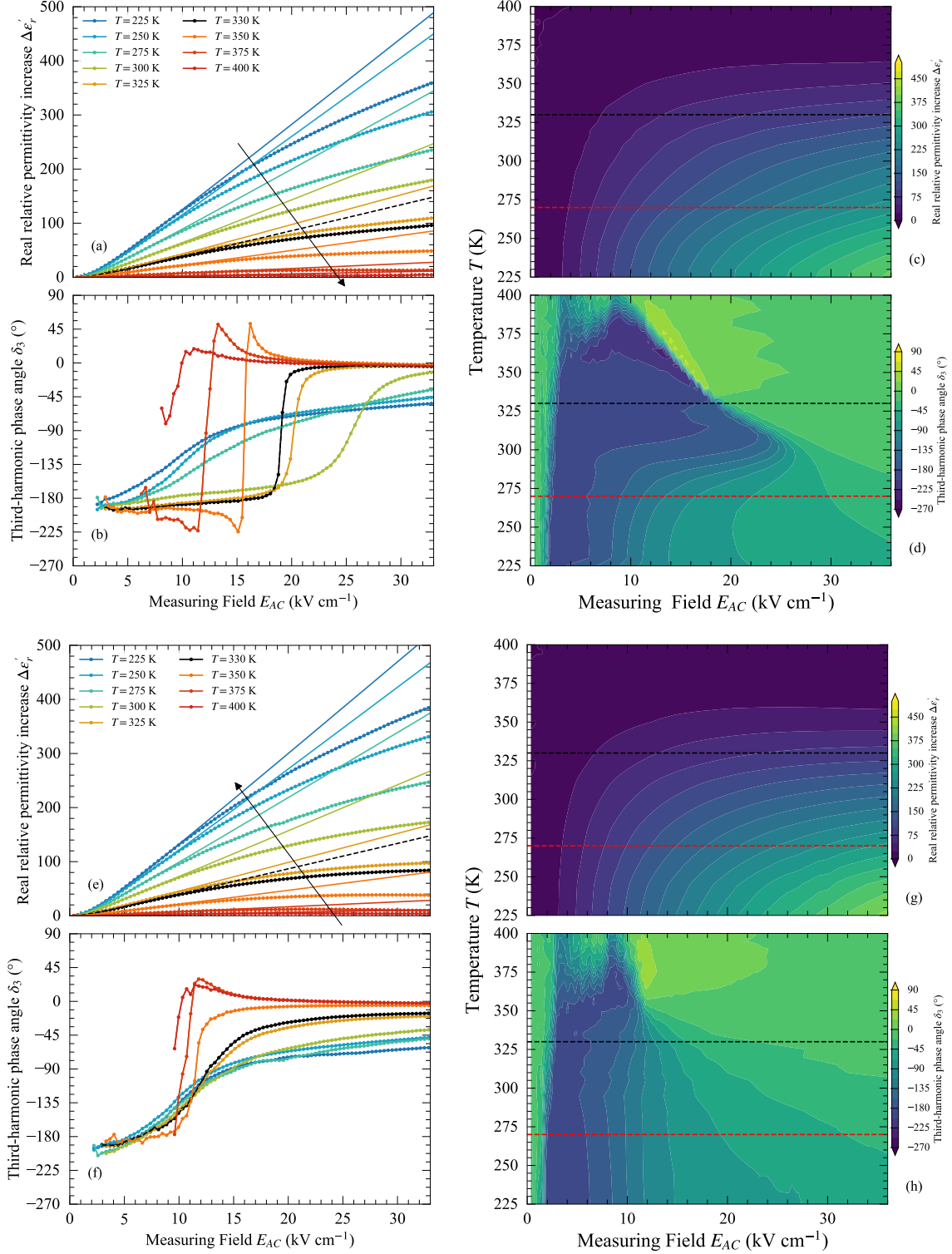


Figure 3. Relative permittivity variation (a,c) and phase angle of the third harmonic (b,d) as a function of the AC measuring field for different values of the temperature, on heating and (e,f,g,h) on cooling. For relative permittivity presented in (a), dots correspond to the experimental data and the solid lines to the hyperbolic fits. The black dashed line corresponds to T_{max} (at $E_{AC} = 0.4$ kV cm⁻¹). The red dashed line in (c,d) corresponds to the inflection point at $T = 270$ K. Data presented in (a,b,e,f) corresponds to slices every 25 K of the data presented in (c,d,g,h).

hard ferroelectrics²⁰: for low AC fields, $\delta_3 \simeq -180^\circ$, then when the AC field increases, δ_3 increases and tends to a limit value around -45° . This transition indicates a flat and random pinning potential for domain walls that can easily move both in reversible and irreversible ways. At low fields, a value of $\delta_3 = -180^\circ$ corresponds to a non-hysteretic contribution of the domain wall motion to the permittivity^{13,30}. This value is found for many ferroelectrics at low AC fields where the reversible domain motion contribution (vibration) dominates^{29,32,33}. At higher fields, the phase angle of the third harmonic evolves toward -90° and corresponds to a purely hysteretic domain wall motion contribution to the permittivity, which results in a linear increase of the permittivity. It is the theoretical Rayleigh behavior. At even higher fields, a saturating-like response is observed with δ_3 around -45° . The evolution of the permittivity for these temperatures (Fig. 3a) also corresponds to what is obtained for soft or weakly hard ferroelectrics: a very limited range for which the permittivity linearly increases (from 3 kV cm^{-1} to 8 kV cm^{-1}) then, the permittivity follows a sublinear increase. When the temperature increases, the phase evolution with the AC field is similar up to 275 K, the main difference resides in the phase-angle value at large fields (33 kV cm^{-1}) which progressively increases.

At 300 K, the phase-angle increases from -180° to -135° and then increases quickly to 0° . This type of phase-angle response is close to the one obtained for relaxors^{13,20,21,30}. A value of $\delta_3 = 0^\circ$ reflects a non-hysteretic contribution, but in that case it corresponds to a saturation of the permittivity. The principal difference with the literature is the presence of a plateau before the increase to 0° which extends to larger electric fields here (20 kV cm^{-1} instead of few kV cm^{-1}). This may be due to the different sample form (thin film here vs ceramics) [similar to Fig. S4 in 21]. At 325 K, the response is quite similar to the one at 300 K, even if the transition from -180° to 0° is sharper.

For temperatures above T_{max} , i.e. above 330 K, the phase-angle response exhibits a peculiar evolution: for low fields the value stays almost constant at -180° but for higher fields instead of a transition by -90° to 0° , the phase-angle decreases and exhibits a negative spike at -225° followed by a positive spike at $+45^\circ$. The crossing of T_{max} and the associated change of regime is well visible on Fig. 3d. This behavior has not been reported in the literature and this abrupt change in the phase-angle can be used to monitor the crossing of T_{max} . A phase-angle of -270° (or $+90^\circ$) indicates a pinching of the hysteresis loop³¹. For the pinching, a value close to -240° is usually observed experimentally because of the competing contribution of the vibration from domain walls ($\delta_3 = -180^\circ$)³⁰. Pinching of the hysteresis loop can have many origins: (i) fresh state for hard ferroelectrics such as Fe-doped $\text{PbZr}_{0.58}\text{Ti}_{0.42}\text{O}_3$ ³¹, (ii) aged state and oxygen vacancies migration for Cu-doped BaTiO_3 ⁵⁸, Ce-doped $\text{Ba}(\text{Ti}_{0.99}\text{Mn}_{0.01})\text{O}_3$ ⁵⁹ or (iii) electric field-induced transition from the paraelectric to a ferroelectric state for

BaTiO_3 ⁶⁰ or $(1-x)(\text{Bi}_{1/2}\text{Na}_{1/2})\text{TiO}_3 - x \text{BaTiO}_3$ ⁶¹. This later could play a role in our measurement since the change occurs near T_{max} and the magnitude of the AC field stays low (and limits aging).

The electric field E_{t1} needed to induce a paraelectric to a ferroelectric state above T_{max} should increase with the temperature^{60,61}. One can note in our case, the electric field $E_{AC}^{-270^\circ}$, for which the phase angle of the third harmonic approaches -270° , decreases from 18 kV cm^{-1} to 12 kV cm^{-1} when the temperature increases from 335 K to 380 K. Thus, the field $E_{AC}^{-270^\circ}$ may not correspond to E_{t1} but to the field for which (i) below, the non-linearity is governed by reversible domain wall contribution ($\delta_3 \simeq -180^\circ$) and (ii) above, the non-linearity is governed by saturation ($\delta_3 \simeq 0^\circ$). Around $E_{AC}^{-270^\circ}$, the deviation from the theoretical value, $\delta_3 = -180^\circ$ for reversible and $\delta_3 = 0^\circ$ for saturation, is attributed to a pinching of the loop and the measured phase corresponds to the combination of the different contributions.³⁰ More explicitly, the negative spike at 225° results from a mix of reversible contributions and pinching, and the positive spike at $+45^\circ$ corresponds to a mix between pinching and saturation.

At high temperatures (for 375 K and especially for 400 K) and low AC field ($E_{AC} < 10 \text{ kV cm}^{-1}$), the non-linearity is so weak ($\Delta\epsilon'_r < 10$) that the phase angle of the third harmonic is difficult to measure resulting in a noisy behavior.

Directly following the measurements on heating, data have been acquired on cooling as well (Fig. 3f). At 375 K, the peculiar behavior ($-180^\circ \rightarrow -225^\circ \rightarrow +45^\circ \rightarrow 0^\circ$) is less visible than on heating. At 350 K, the peculiar behavior is not observed and instead the phase angle of the third harmonic evolution corresponds to a conventional relaxor behavior. At T_{max} (330 K), the phase response corresponds to a relaxor but with a smoother transition from -180° to 0° compared to data on heating. Below 300 K, the phase evolution corresponds to a conventional ferroelectric with high field asymptotes from -30° to -70° .

These differences indicate that the domain structure (domains, domain walls, polar cluster boundaries, phase boundaries, etc) is different on heating and on cooling. Such difference can already be inferred from $P(E)$ hysteresis loops (see Fig. S6b in supplementary material). At 225 K, they exhibit a horizontal shift, characteristic of an internal field with a value around 12 kV cm^{-1} . It increases to around 14 kV cm^{-1} at 300 K and then decreases with increasing temperatures. We postulate that this internal field indicates some correlations between PNRs, that would decrease with thermal fluctuations at higher temperatures. On cooling, the internal field is smaller (as low as 6 kV cm^{-1}) until 325 K, implying that the correlations between PNRs are weaker. In the dielectric measurements we perform, at low temperatures, the application of the AC field may increase correlations between PNRs^{62,63}. When the temperature increases, close to the phase transition, the correlation between the PNRs de-

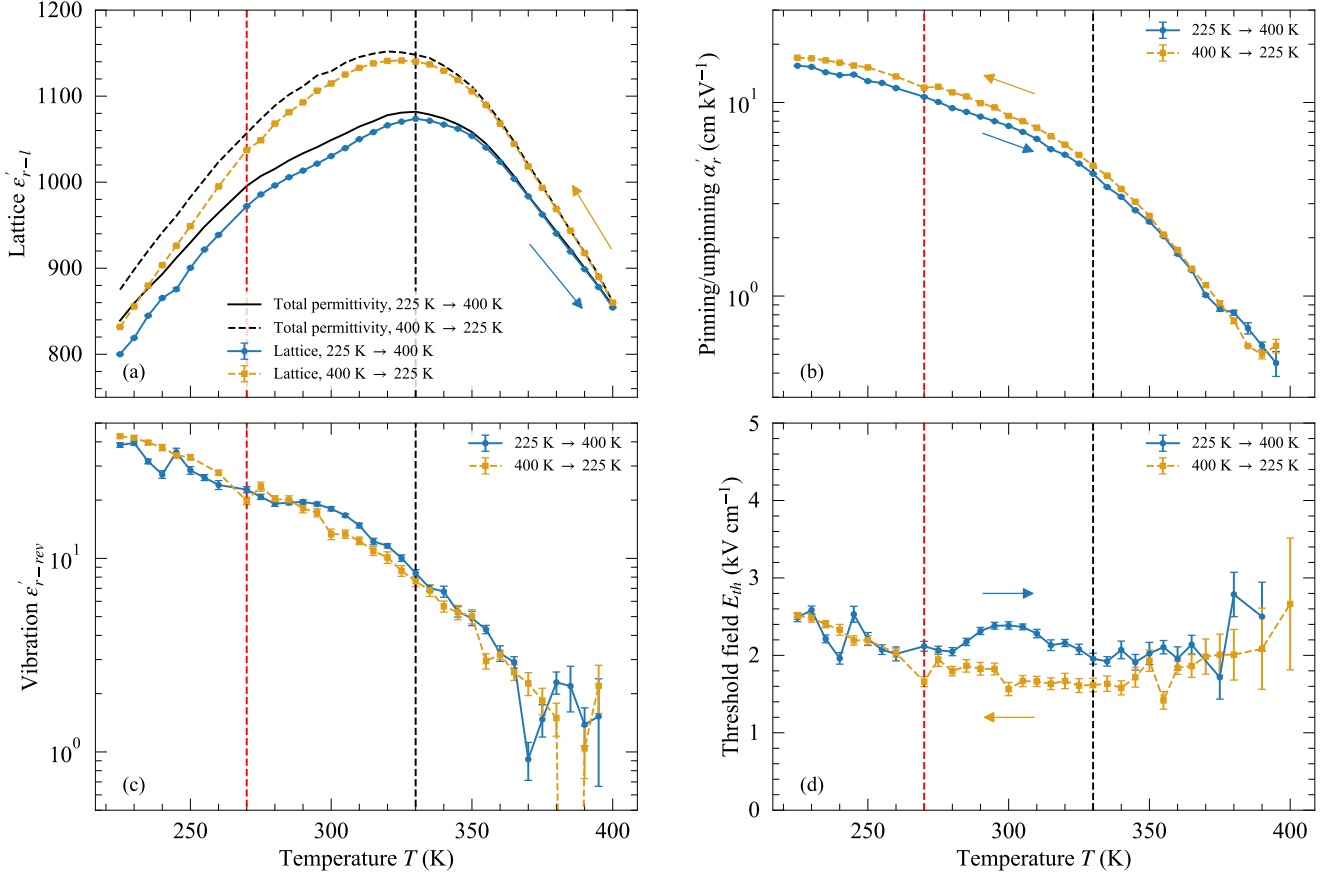


Figure 4. Relative permittivity for a measuring field of 0.4 kV cm^{-1} , lattice contribution to the permittivity (a), domain wall motion contributions to the permittivity (b,c) and threshold field (d) as a function of the temperature.

creases due to thermal fluctuation (the internal bias field decreases) but when the AC field is applied, they can be correlated again, creating a pinching, i.e. a phase angle of the third harmonic approaching 270° . On cooling, the domain structure is different and most PNRs are uncorrelated since above the transition, the conventional relaxor behavior is observed and the AC field is not enough to induce pinching. On cooling further, PNRs stay less correlated and thus the global response of the material probed using AC field is closer to a conventional ferroelectric response.

The real part of the permittivity measurement as a function of the AC measuring field has been fitted using (4) and Levenberg-Marquat algorithm and the resulting fits are shown as solid lines (Fig. 3a). Only the data below 7 kV cm^{-1} have been used for the fit since a deviation from the Rayleigh law occurs at higher fields. The hyperbolic fits values are given in Fig. 4 as a function of the temperature, with associated confidence intervals. The lattice contribution shows a similar evolution with temperature as the total permittivity, consistent with the fact that, at low fields, it represents the main contribution to the permittivity. Its maximum occurs for 334 K,

very close to the T_{max} found at low fields (330 K). The slight difference below T_{max} correspond to the reversible domain wall motion contribution.

Fig. 4b,c show the domain wall motion contributions to the permittivity. There are no measurements in the literature on thin films of BCTZ. Still it is useful to compare with room temperature measurements on ceramics where α_r is around 300 cm kV^{-1} to 3000 cm kV^{-1} ^{64–66}, much larger than the values we find here. This indicates that domain walls are less mobile in thin films which is attributed to clamping of the film⁶⁷.

Below T_{max} , both domain wall motion contributions decrease when the temperature increases, without any change at 270 K where there was an inflection point in the real part of the permittivity. This differs from what has been found for films of $(\text{Pb,Sr})\text{TiO}_3$ ³⁶ or $0.5\text{PbYb}_{1/2}\text{Nb}_{1/2}-0.5\text{PbTiO}_3$ ³³ for which the domain wall motion contribution increases when the temperature approaches T_{max} . Above T_{max} , the domain wall motion coefficients still decrease but are not null, corresponding to a residual ferroelectricity^{17,18}, which persists here 70 K above T_{max} . The decrease is slightly more pronounced than before: at 330 K α'_r is 3 times lower than

at 260 K whereas at 400 K, α'_r is 9 times lower than a 330 K. The change of decay rate is also visible on the reversible contribution. According to Boser³⁷, the reversible domain wall contribution is proportional to the domain wall density and the distance traveled by the domain wall, this later depending on the potential energy profile of the domain wall³³. A stronger decrease of the reversible contribution could thus indicate faster changes in the density of domain walls, which would be consistent with the fact that above T_{max} the number of PNRs and their sizes both decrease.^{46,68} In the studied sample, the reversible and irreversible contributions do not exhibit a peak, contrary to what has been seen for NaNbO_3 ⁵⁴, $\text{Pb}_{0.92}\text{La}_{0.08}\text{Zr}_{0.52}\text{Ti}_{0.48}\text{O}_3$ ⁴⁶, Nb-doped PbZrO_3 ⁶⁸ or $\text{PbMn}_{1/3}\text{Nb}_{2/3}\text{O}_3$ ⁵⁶.

One can note that the reversible domain wall contribution fluctuates above 350 K because the non-linearity becomes very weak above T_{max} and makes the coefficient extraction using (4) difficult. The confidence intervals in absolute values are similar for the lattice contribution and the reversible contribution (mean value of 0.6). This effect is accentuated by the semi-log scale

Using reversible and irreversible domain wall motion contributions, it is possible to determine the threshold field $E_{th} = \varepsilon'_{r-rev}/\alpha'_r$ which represents the degree of pinning of the domain walls^{34,39,42}. The threshold field remains almost constant when the temperature changes, indicating a constant degree of pinning. This suggests that the decrease of the non-linear behavior, i.e. the irreversible domain wall motion contribution, with increasing temperature results from a decrease of the domain wall density and not a change in energy profile. The fluctuation at temperatures above 350 K results from fluctuations of the reversible domain wall motions contribution.

When repeating the measurement on cooling, the lattice contribution is slightly higher (similar to what is found for the total permittivity). The irreversible domain wall contribution is also slightly higher (15%) indicating a higher non-linear behavior. Since the reversible domain wall contribution is similar on cooling and on heating, the higher irreversible contribution is due to higher domain wall mobility, which is confirmed by a small value of the threshold field on cooling.

In summary, in this article, we studied the sub-coercive field non-linearities as a function of the temperature of a BCTZ 50/50 thin film. The relaxor behavior of the film is confirmed by the shift of the maximum permittivity temperature T_{max} with frequency and the slim shape of the $P(E)$ loops. We have shown that T_{max} also depends on the AC measuring field because of the irreversible domain wall motion contribution. The domain wall contributions is found to regularly decrease with temperature and still contribute to the permittivity above T_{max} . In addition, phase angle of the third harmonic measurements show that the thin film behaves like a conventional ferroelectric below 275 K and as a relaxor from 275 K to $T_{max} = 330$ K. Above T_{max} , the thin film exhibits a peculiar phase angle of the third harmonic response which

consists of $-180^\circ \rightarrow -225^\circ \rightarrow +45^\circ \rightarrow 0^\circ$ instead of the $-180^\circ \rightarrow -90^\circ \rightarrow 0^\circ$ found for relaxor. This peculiar behavior is observed only on heating, and is tentatively attributed to changes in the correlations between polar nanoregions.

SUPPLEMENTARY MATERIAL

The thin film growth procedure, the associated phase/composition characterizations, polarization versus electric field loop and modified Curie-Weiss analysis are given in supplementary material.

DATA AVAILABILITY

The data that support the findings of this study are available from the corresponding author upon reasonable request.

ACKNOWLEDGMENTS

This work has been performed with the means of the CERTeM (microelectronics technological research and development center) of French region Centre Val de Loire. This work was funded through the project MAPS in the program ARD+ CERTeM 5.0 by the Région Centre Val de Loire co-funded by the European Union (ERC, DYNAMHEAT, N°101077402). Views and opinions expressed are however those of the authors only and do not necessarily reflect those of the European Union or the European Research Council. Neither the European Union nor the granting authority can be held responsible for them.

The authors would like to thank Brahim Dkhil for fruitful discussions on the relaxor behavior.

CONFLICT OF INTEREST

The authors declare no competing financial interest.

REFERENCES

- ¹A. Jayakrishnan, J. Silva, K. Kamakshi, D. Dastan, V. Annappureddy, M. Pereira, and K. Sekhar, *Progress in Materials Science* **132**, 101046 (2023).
- ²V. Veerapandiyam, F. Benes, T. Gindel, and M. Deluca, *Materials* **13**, 5742 (2020).
- ³Q. Simon, C. J. M. Daumont, S. Payan, P. Gardes, P. Poveda, J. Wolfman, and M. Maglione, *Journal of Alloys and Compounds* **747**, 366 (2018).
- ⁴C. J. M. Daumont, Q. Simon, E. Le Mouellic, S. Payan, P. Gardes, P. Poveda, B. Negulescu, M. Maglione, and J. Wolfman, *Journal of Applied Physics* **119**, 094107 (2016), publisher: American Institute of Physics.

- ⁵V. S. Puli, D. K. Pradhan, I. Coondoo, N. Panwar, S. Adireddy, S. Luo, R. S. Katiyar, and D. B. Chrisey, *Journal of Physics D: Applied Physics* **52**, 255304 (2019).
- ⁶X. Yan, M. Zheng, X. Gao, M. Zhu, and Y. Hou, *Journal of Materials Chemistry C* **8**, 13530 (2020).
- ⁷M. Zheng, C. Zhao, X. Yan, R. Khachatryan, F. Zhuo, Y. Hou, and J. Koruza, *Advanced Functional Materials* (2023), [10.1002/adfm.202301356](https://doi.org/10.1002/adfm.202301356).
- ⁸M. A. Carpenter, *Journal of Physics: Condensed Matter* **27**, 263201 (2015).
- ⁹D. Damjanovic, *Journal of the American Ceramic Society* **88**, 2663 (2005).
- ¹⁰E. V. Colla, N. K. Yushin, and D. Viehland, *Journal of Applied Physics* **83**, 3298 (1998), publisher: American Institute of Physics.
- ¹¹R. Cowley, S. Gvasaliya, S. Lushnikov, B. Roessli, and G. Rotaru, *Advances in Physics - ADVAN PHYS* **60**, 229 (2011).
- ¹²A. A. Bokov and Z.-G. Ye, *Journal of Materials Science* **41**, 31 (2006).
- ¹³M. Otoničar, A. Bradeško, L. Fulanović, T. Kos, H. Uršič, A. Benčan, M. J. Cabral, A. Henriques, J. L. Jones, L. Riemer, D. Damjanovic, G. Dražić, B. Malič, and T. Rojac, *Advanced Functional Materials* **30**, 2006823 (2020), [_eprint: https://onlinelibrary.wiley.com/doi/pdf/10.1002/adfm.202006823](https://onlinelibrary.wiley.com/doi/pdf/10.1002/adfm.202006823).
- ¹⁴F. Li, S. Zhang, T. Zhang, Z. Xu, N. Zhang, G. Liu, J. Wang, J. Wang, Z. Cheng, Z.-G. Ye, J. Luo, T. R. Shrout, and L.-Q. Chen, *Nature Communications* **7** (2016), [10.1038/ncomms13807](https://doi.org/10.1038/ncomms13807).
- ¹⁵F. Li, S. Zhang, D. Damjanovic, L.-Q. Chen, and T. R. Shrout, *Advanced Functional Materials* **28**, 1801504 (2018), [_eprint: https://onlinelibrary.wiley.com/doi/pdf/10.1002/adfm.201801504](https://onlinelibrary.wiley.com/doi/pdf/10.1002/adfm.201801504).
- ¹⁶F. Li, S. Zhang, Z. Xu, and L.-Q. Chen, *Advanced Functional Materials* **27**, 1700310 (2017).
- ¹⁷L. M. Garten, M. Burch, A. S. Gupta, R. Haislmaier, V. Gopalan, E. C. Dickey, and S. Trolier-McKinstry, *Journal of the American Ceramic Society* **99**, 1645 (2016).
- ¹⁸L. M. Garten, P. Lam, D. Harris, J.-P. Maria, and S. Trolier-McKinstry, *Journal of Applied Physics* **116**, 044104 (2014).
- ¹⁹E. K. H. Salje, M. A. Carpenter, G. F. Nataf, G. Picht, K. Weber, J. Weerasinghe, S. Lisenkov, and L. Bellaiche, *Physical Review B* **87** (2013), [10.1103/physrevb.87.014106](https://doi.org/10.1103/physrevb.87.014106).
- ²⁰M. Otoničar, M. Dragomir, and T. Rojac, *Journal of the American Ceramic Society* **105** (2022), [10.1111/jace.18623](https://doi.org/10.1111/jace.18623).
- ²¹S. Hashemizadeh and D. Damjanovic, *Applied Physics Letters* **110**, 192905 (2017).
- ²²T. Maiti, R. Guo, and A. S. Bhalla, *Ferroelectrics* **425**, 4 (2011).
- ²³G. Burns and B. Scott, *Solid State Communications* **13**, 417 (1973).
- ²⁴R. Pirc and R. Blinc, *Physical Review B* **76** (2007), [10.1103/physrevb.76.020101](https://doi.org/10.1103/physrevb.76.020101).
- ²⁵B. Dkhil and J. M. Kiat, *Journal of Applied Physics* **90**, 4676 (2001).
- ²⁶I. P. Raevski, S. A. Prosandeev, A. S. Emelyanov, S. I. Raevskaya, E. V. Colla, D. Viehland, W. Kleemann, S. B. Vakhrushev, J.-L. Dellis, M. E. Marssi, and L. Jastrabik, *Physical Review B* **72** (2005), [10.1103/physrevb.72.184104](https://doi.org/10.1103/physrevb.72.184104).
- ²⁷S. Prosandeev, D. Wang, A. R. Akbarzadeh, B. Dkhil, and L. Bellaiche, *Physical Review Letters* **110** (2013), [10.1103/physrevlett.110.207601](https://doi.org/10.1103/physrevlett.110.207601).
- ²⁸D. V. Taylor and D. Damjanovic, *Journal of Applied Physics* **82**, 1973 (1997).
- ²⁹T. Schenk, M. Hoffmann, M. Pešić, M. H. Park, C. Richter, U. Schroeder, and T. Mikolajick, *Physical Review Applied* **10**, 064004 (2018).
- ³⁰L. M. Riemer, L. Jin, H. Uršič, M. Otoničar, T. Rojac, and D. Damjanovic, *Journal of Applied Physics* **129**, 054101 (2021).
- ³¹M. I. Morozov and D. Damjanovic, *Journal of Applied Physics* **104**, 034107 (2008).
- ³²K. Nadaud, C. Borderon, R. Renoud, M. Bah, S. Ginestar, and H. W. Gundel, *Journal of Applied Physics* **133** (2023), [10.1063/5.0143659](https://doi.org/10.1063/5.0143659).
- ³³N. Bassiri-Gharb, I. Fujii, E. Hong, S. Trolier-McKinstry, D. V. Taylor, and D. Damjanovic, *Journal of Electroceramics* **19**, 49 (2007).
- ³⁴C. Borderon, R. Renoud, M. Ragheb, and H. W. Gundel, *Applied Physics Letters* **98**, 112903 (2011).
- ³⁵K. Nadaud, C. Borderon, R. Renoud, M. Bah, S. Ginestar, and H. W. Gundel, *Applied Physics Letters* **118**, 042902 (2021).
- ³⁶J. Bai, J. Yang, Y. Zhang, W. Bai, Z. Lv, K. Tang, J. Sun, X. Meng, X. Tang, and J. Chu, *Ceramics International* **43**, S516 (2017).
- ³⁷O. Boser, *Journal of Applied Physics* **62**, 1344 (1987).
- ³⁸K. Nadaud, M. Sadl, M. Bah, F. Levassort, and H. Ursic, *Applied Physics Letters* **120**, 112902 (2022).
- ³⁹C. Borderon, A. E. Brunier, K. Nadaud, R. Renoud, M. Alexe, and H. W. Gundel, *Scientific Reports* **7**, 3444 (2017).
- ⁴⁰R. Renoud, C. Borderon, and H. Gundel, *Ultrasonics, Ferroelectrics, and Frequency Control, IEEE Transactions on* **58**, 1975 (2011).
- ⁴¹K. Nadaud, C. Borderon, R. Renoud, and H. W. Gundel, *Journal of Applied Physics* **119**, 114101 (2016).
- ⁴²N. B. Gharb and S. Trolier-McKinstry, *Journal of Applied Physics* **97**, 064106 (2005).
- ⁴³D. Ghosh, A. Sakata, J. Carter, P. A. Thomas, H. Han, J. C. Nino, and J. L. Jones, *Advanced Functional Materials* **24**, 885–896 (2013).
- ⁴⁴K. Nadaud, C. Borderon, R. Renoud, A. Ghalem, A. Crunteanu, L. Huitema, F. Dumas-Bouchiat, P. Marchet, C. Champeaux, and H. W. Gundel, *Applied Physics Letters* **112**, 262901 (2018).
- ⁴⁵K. Nadaud, C. Borderon, R. Renoud, M. Bah, S. Ginestar, and H. W. Gundel, *Journal of Alloys and Compounds* **914**, 165340 (2022).
- ⁴⁶B. Ma, Z. Hu, S. Liu, S. Tong, M. Narayanan, R. E. Koritala, and U. Balachandran, *Applied Physics Letters* **102**, 202901 (2013).
- ⁴⁷D. Damjanovic, A. Biancoli, L. Batooli, A. Vahabzadeh, and J. Trodahl, *Applied Physics Letters* **100**, 192907 (2012).
- ⁴⁸F. Feng and Y. Yan, *Ceramics International* **45**, 21315 (2019).
- ⁴⁹M. Gao, W. Ge, X. Li, H. Yuan, C. Liu, H. Zhao, Y. Ma, and Y. Chang, *physica status solidi (a)* **217**, 2000253 (2020), [_eprint: https://onlinelibrary.wiley.com/doi/pdf/10.1002/pssa.202000253](https://onlinelibrary.wiley.com/doi/pdf/10.1002/pssa.202000253).
- ⁵⁰X. Liu, Y. Dai, X. Pei, and W. Chen, *Ceramics International* **49**, 1846 (2023).
- ⁵¹X. Xu, G. Yuan, B. Xu, J. Yin, J. Liu, and Z. Liu, *Journal of the American Ceramic Society* **98**, 2823 (2015).
- ⁵²A. B. Haugen, J. S. Forrester, D. Damjanovic, B. Li, K. J. Bowman, and J. L. Jones, *Journal of Applied Physics* **113** (2013), [10.1063/1.4772741](https://doi.org/10.1063/1.4772741).
- ⁵³F. Benabdallah, A. Simon, H. Khemakhem, C. Elissalde, and M. Maglione, *Journal of Applied Physics* **109** (2011), [10.1063/1.3599854](https://doi.org/10.1063/1.3599854).
- ⁵⁴B. Cai, J. Schwarzkopf, E. Hollmann, D. Braun, M. Schmidbauer, T. Grellmann, and R. Wördenweber, *Physical Review B* **93**, 224107 (2016), publisher: American Physical Society.
- ⁵⁵E. V. Colla, E. L. Furman, S. M. Gupta, N. K. Yushin, and D. Viehland, *Journal of Applied Physics* **85**, 1693 (1999).
- ⁵⁶S. Shetty, A. Damodaran, K. Wang, Y. Yuan, V. Gopalan, L. Martin, and S. Trolier-McKinstry, *Advanced Functional Materials* **29**, 1804258 (2019), [_eprint: https://onlinelibrary.wiley.com/doi/pdf/10.1002/adfm.201804258](https://onlinelibrary.wiley.com/doi/pdf/10.1002/adfm.201804258).
- ⁵⁷L. M. Garten and S. Trolier-McKinstry, *Applied Physics Letters* **105**, 132905 (2014), [10.1063/1.4897299](https://doi.org/10.1063/1.4897299).
- ⁵⁸Z. Li, J. Yu, S. Hao, and P.-E. Janolin, *Journal of the European Ceramic Society* **42**, 4693 (2022).
- ⁵⁹Y. Zhao, J. Wang, L. Zhang, C. Wang, and S. Liu, *Ceramics International The 10th Asian Meeting on Electroceramics (AMEC-10)*, **43**, S70 (2017).
- ⁶⁰W. J. Merz, *Physical Review* **91**, 513 (1953).
- ⁶¹E. Sapper, N. Novak, W. Jo, T. Granzow, and J. Rödel, *Journal of Applied Physics* **115**, 194104 (2014).
- ⁶²C. Qiu, J. Liu, F. Li, and Z. Xu, **125**, 014102.

- ⁶³G. Tian, F. Liu, J. Du, L. Zhao, X. Qi, M. Zhao, and L. Zheng, **122**, 102901.
- ⁶⁴Y. Liu, Y. Chang, F. Li, B. Yang, Y. Sun, J. Wu, S. Zhang, R. Wang, and W. Cao, *ACS Applied Materials & Interfaces* **9**, 29863 (2017).
- ⁶⁵M. Abebe, K. Brajesh, and R. Ranjan, *Journal of Applied Physics* **122** (2017), 10.1063/1.4990119.
- ⁶⁶M. Zheng, C. Zhao, and J. Rödel, *Applied Physics Letters* **122** (2023), 10.1063/5.0146096.
- ⁶⁷R. Keech, S. Shetty, M. A. Kuroda, X. Hu Liu, G. J. Martyna, D. M. News, and S. Trolier-McKinstry, *Journal of Applied Physics* **115**, 234106 (2014).
- ⁶⁸M. Ye, H. Huang, T. Li, S. Ke, P. Lin, B. Peng, M. Mai, Q. Sun, X. Peng, and X. Zeng, *Applied Physics Letters* **107**, 202902 (2015).